A Discretization of the Wave Field Synthesis Method for Auralization of Natural Sounds

César D. Salvador[1, 2]
salvador.cd@pucp.edu.pe
[1]Pontificia Universidad Católica del Perú
Av. Universitaria 1801, San Miguel, Lima 31 Perú
[2]Universidad de San Martin de Porres
Av. Tomás Marsano 155, Surquillo, Lima 34 Perú

ABSTRACT

A complete description of the implementation of an immersive soundscape is proposed in this document. It begins with the time-discretization of the continuous wave field synthesis method for arbitrary contours, with special attention to the pre-filter stage that involves a fractional order system. On this stage, the Al-alaoui discretization, the Grünwald-Letnikov approach for fractional expansion, and the Shank least squares approximation method to compute the zero-pole filter that generates the fractional system are described. The document goes on to explain the rendering of background and foreground sounds, using respectively plane and spherical wave models. The simulations of sound pressure fields inside the listening area also shown. Finally, simulations of a real case report a discretization percentage error around 1%, using 24 loudspeakers and a 5th order IIR pre-filter per channel.

Keywords: Wave field synthesis, fractional order systems, loudspeaker array, soundscapes.

1. INTRODUCTION

Wave field synthesis (WFS) is a physics-based sound reproduction technique [1], [2]. It allows the synthesis of wave fronts that appear to emanate from a virtual source at a defined position. WFS provides the listener consistent spatial localization cues over an extended listening area, but it utilizes a high number of loudspeakers as secondary sources to recreate a virtual acoustic environment. On the other hand, the concept of soundscape, introduced by Schafer [3], refers to both the natural acoustic environment and the sounds created by humans. The study of soundscape is the subject of acoustic ecology which main field method is the recording and classification of sounds according to its quality and social significance. Actually, the soundscape and sound art community have special attention on virtual auditory scenes due to its capability to recreate the original recording scene. It promotes in this way awareness of acoustical ecology and enhances the interaction between the subject and the piece of art due to its immersive scenery.

This document reports a procedure to render natural sounds towards the composition of an immersive soundscape. The technical motivation for this work is that a discrete-time representation in terms of IIR filters of the continuous WFS driving functions is very useful given that most of real time DSP environments include zero-pole filters in their libraries. Section 2 explains how to map the continuous WFS model to a discrete representation suitable for a real time implementation. Section 3 evaluates some loudspeaker distribution in order to select a suitable contour shape of loudspeakers array. Section 4 briefly describes the considerations for sound recording, with special attention in its upcoming real time auralization as foreground and background sounds. Section 5 presents a practical example of an immersive soundscape composition. Finally, conclusions and comments on the actual stage of this work are stated.

2. A DISCRETE ZERO-POLE WAVE FIELD SYNTHESIS FORMULATION

Following the revisited wave field synthesis method described in [4] (see figure 1), the wave field emanating from the virtual source at $\mathbf{x_s} = [x_s \; y_s]^\mathbf{T}$ can be synthesized in the listening area enclosed by an arbitrary contour ∂V using loudspeakers at $\mathbf{x_0} = [x_0 \; y_0]^\mathbf{T}$ along this contour as secondary sources. The normal vector to ∂V at $\mathbf{x_0}$ is the column $\mathbf{n}(\mathbf{x_0})$ and the reference position is $\mathbf{x_{ref}} = [x_{ref} \; y_{ref}]^\mathbf{T}$.

The driving function of a loudspeaker at $\mathbf{x_0}$, for the synthesis of a plane wave $S_{\mathrm{PW}}(\mathbf{x}, \omega) = \hat{S}_{\mathrm{PW}}(\omega)\exp(-j\omega \mathbf{n}_{\mathrm{PW}}^T \mathbf{x}/c)$, with spectrum $\hat{S}_{\mathrm{PW}}(\omega)$ propagating in the $\mathbf{n}_{\mathrm{PW}}$ direction, is

$$D_{\mathrm{PW,2.5D}}(\mathbf{x_0}, \omega) = -2a_{\mathrm{PW}}(\mathbf{x_0})\sqrt{2\pi|\mathbf{x_{ref}} - \mathbf{x_0}|}\,\mathbf{n}_{\mathrm{PW}}^T\mathbf{n}(\mathbf{x_0}) \times \frac{1}{\sqrt{c}}(j\omega)^{1/2} e^{-j\omega\frac{\mathbf{n}_{\mathrm{PW}}^T\mathbf{x_0}}{c}} \hat{S}_{\mathrm{PW}}(\omega), \quad (1)$$

where, $|\cdot|$ denotes the Euclidian norm, c is the velocity of sound in air, and the selection loudspeaker functions is

$$a_{\mathrm{PW}}(\mathbf{x_0}) = \begin{cases} 1 & \text{, if } \mathbf{n}_{\mathrm{PW}}^T\mathbf{n}(\mathbf{x_0}) > 0, \\ 0 & \text{, otherwise.} \end{cases} \quad (2)$$

The driving function for the synthesis of the spherical wave $S_{\mathrm{SW}}(\mathbf{x}, \omega) = \hat{S}_{\mathrm{SW}}(\omega)\exp(-j\omega|\mathbf{x} - \mathbf{x_s}|/c)/|\mathbf{x} - \mathbf{x_s}|$ with spectrum $\hat{S}_{\mathrm{SW}}(\omega)$ emanating from $\mathbf{x_s}$, is

$$D_{SW,2.5D}(\mathbf{x_0}, \omega) = -2a_{SW}(\mathbf{x_0})\sqrt{2\pi|\mathbf{x_{ref}} - \mathbf{x_0}|}\,\frac{(\mathbf{x_0} - \mathbf{x_s})^T\mathbf{n}(\mathbf{x_0})}{|\mathbf{x_0} - \mathbf{x_s}|^2} \times \frac{1}{\sqrt{c}}\left(j\omega + \frac{c}{|\mathbf{x_0} - \mathbf{x_s}|}\right)(j\omega)^{-1/2} e^{-j\omega\frac{|\mathbf{x_0} - \mathbf{x_s}|}{c}} \hat{S}_{SW}(\omega), \quad (3)$$

where the loudspeaker selection function is:

$$a_{\mathrm{SW}}(\mathbf{x_0}) = \begin{cases} 1 & \text{, if } (\mathbf{x_0} - \mathbf{x_s})^T\mathbf{n}(\mathbf{x_0}) > 0, \\ 0 & \text{, otherwise.} \end{cases} \quad (4)$$

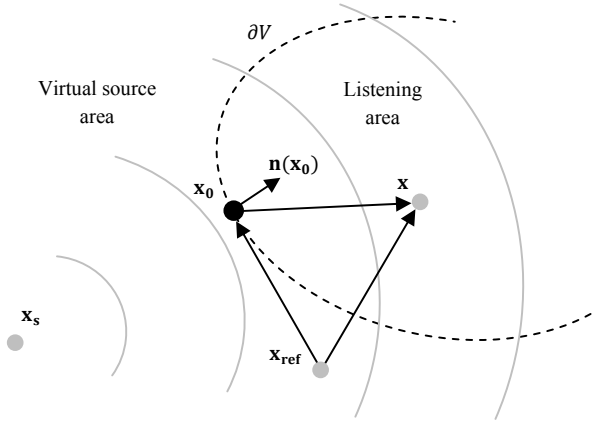

Figure1. The geometry used in wave field synthesis (from [4]).

Equations (1) and (3) show that the rendering of plane and spherical waves requires respectively half order differentiation and integration. A continuous to discrete map at a sampling rate F_s is calculated with the Al-alaoui approximation $j\omega \approx (8F_s/7)\,(1-z^{-1})/(1+1/7\,z^{-1})$, which corresponds to an interpolation between the Euler and Tustin approximations [5], [6]. At this point, the power series expansion of the result is

$$(j\omega)^{\alpha} \approx \left(\frac{8F_s}{7}\frac{1-z^{-1}}{1+\frac{1}{7}z^{-1}}\right)^{\alpha} \approx \sum_{k=0}^{K} h(k)z^{-k}. \tag{5}$$

Following the Grünwald-Letnikov approach for fractional integration and differentiation, we can compute the Taylor series of the middle term [7]. The coefficients of the $K+1$ order polynomial in z now is

$$h(k) = \left(\frac{8F_s}{7}\right)^{\alpha} \sum_{j=0}^{k} (-1)^j \left(\frac{1}{7}\right)^{k-j} \binom{\alpha}{j}\binom{-\alpha}{k-j} \tag{6}$$

where $\binom{\alpha}{j} = \frac{\Gamma(\alpha+1)}{\Gamma(j+1)\Gamma(\alpha-j+1)}$ is the generalization of the binomial function for rational numbers, and $\Gamma(\alpha) = \int_0^{\infty} t^{\alpha-1}e^{-t}dt$ is the gamma function: an interpolation that extents the factorial function to rational numbers. Since the later polynomial representation corresponds to a very large FIR filter, it is preferable to transform it into a short IIR filter as follows:

$$(j\omega)^{\alpha} \approx \sum_{k=0}^{K} h(k)z^{-k} = \frac{\sum_{k=0}^{m} b(k)z^{-k}}{1+\sum_{k=1}^{n} a(k)z^{-k}} = g\,\frac{(1-\zeta_1 z^{-1})(1-\zeta_2 z^{-1})\dots(1-\zeta_m z^{-1})}{(1-\pi_1 z^{-1})(1-\pi_2 z^{-1})\dots(1-\pi_n z^{-1})}. \tag{7}$$

To compute the numerator and denominator from $h(k)$ the Shank's method for least squares approximation is used [8], [9]. The idea is to interpret $b(k)$ as the convolution $(h * a)(k)$. Once the associated Toeplitz matrix is identified, its lower half matrix is taken; and $\mathbf{a} = [a(1) \quad a(2) \quad \dots \quad a(n)]^{\mathbf{T}}$ is first computed from $\mathbf{h_2} = [h(m+1) \quad h(m+2) \quad \dots \quad h(N-1)]^{\mathbf{T}}$ with the following pseudo inverse matrix:

$$\mathbf{a} = -\left(\mathbf{H}_2^T\mathbf{H}_2\right)^{-1}\mathbf{H}_2^T\mathbf{h}_2, \tag{8}$$

where

$$\mathbf{H_2} = \begin{bmatrix} h(m) & h(m-1) & \cdots & h(m-n+1) \\ h(m+1) & h(m) & \dots & h(m-n+2) \\ \vdots & \vdots & \ddots & \vdots \\ h(N-2) & h(N-3) & \dots & h(N-n-1) \end{bmatrix}.$$

The next step is to compute the impulse response of the filter $1/(1+\sum_{k=1}^{n} a(k)z^{-k})$, denoted $g(k) = \delta(k) - \sum_{l=1}^{n} a(l)g(k-l)$, $k = 0,1,\dots,N-1$. With this impulse response, a new pseudo inverse matrix appears to compute $\mathbf{b} = [b(0) \quad b(2) \quad \dots \quad b(m)]^{\mathbf{T}}$ from $\mathbf{h} = [h(0) \quad h(1) \quad \dots \quad h(N-1)]^{\mathbf{T}}$ as follows:

$$\mathbf{b} = (\mathbf{G}^{\mathbf{T}}\mathbf{G})^{-1}\mathbf{G}^{\mathbf{T}}\mathbf{h}, \tag{9}$$

where

$$\mathbf{G} = \begin{bmatrix} g(0) & 0 & \cdots & 0 \\ g(1) & g(0) & \dots & 0 \\ \vdots & \vdots & \ddots & \vdots \\ g(N-1) & g(N-2) & \dots & g(N-m-1) \end{bmatrix}.$$

Time delays in equations (1) and (3) are discretize with the map $z = \exp(j\omega/F_s)$. As fractional delays are beyond the scope of this paper, only simulations for rounded delays are reported. To discretize the variable zero in equation (3) the Al-alaoui approximation has also been used. After a proper ordering of factors, a discrete version of the driving functions for plane and spherical waves appears respectively in equations (10) and (11), which is preferable to state in gain-zero-pole form, due to that most of real time DSP environments include zero-pole filters.

The discrete driving function for a plane wave is

$$D_{\mathrm{PW,2.5D}}(\mathbf{x_0}, z) = T_{\mathrm{PW}}(z)A_{\mathrm{PW}}P_{\mathrm{PW}}(z)\hat{S}(z), \tag{10}$$

where

$$P_{\mathrm{PW}}(z) = \frac{g}{\sqrt{c}}\frac{(1-\zeta_1 z^{-1})(1-\zeta_2 z^{-1})\dots(1-\zeta_m z^{-1})}{(1-\pi_1 z^{-1})(1-\pi_2 z^{-1})\dots(1-\pi_n z^{-1})},$$

$$A_{\mathrm{PW}}(\mathbf{x_0}) = -2a_{\mathrm{PW}}(\mathbf{x_0})\sqrt{2\pi|\mathbf{x_{ref}} - \mathbf{x_0}|}\,\mathbf{n}_{\mathrm{PW}}^T\mathbf{n}(\mathbf{x_0}),$$

$$T_{\mathrm{PW}}(\mathbf{x_0}, z) = z^{-\left[\!\left[F_s\frac{\mathbf{n}_{\mathrm{PW}}^T\mathbf{x_0}}{c}\right]\!\right]}.$$

The discrete driving function for a spherical wave is

$$D_{\mathrm{SW,2.5D}}(\mathbf{x_0}, z) = T_{\mathrm{SW}}(z)A_{\mathrm{SW}}F_{\mathrm{SW}}(z)P_{\mathrm{SW}}(z)\hat{S}(z), \tag{11}$$

where

$$P_{\mathrm{SW}}(z) = \frac{g}{\sqrt{c}}\frac{(1-\zeta_1 z^{-1})(1-\zeta_2 z^{-1})\dots(1-\zeta_m z^{-1})}{(1-\pi_1 z^{-1})(1-\pi_2 z^{-1})\dots(1-\pi_n z^{-1})},$$

$$F_{\mathrm{SW}}(\mathbf{x_0}, z) = \frac{1-\frac{|\mathbf{x_0}-\mathbf{x_s}| - \frac{c}{8F_s}}{|\mathbf{x_0}-\mathbf{x_s}| + \frac{7c}{8F_s}}z^{-1}}{1+\frac{1}{7}z^{-1}},$$

$$A_{\mathrm{SW}}(\mathbf{x_0}) = -2a_{\mathrm{SW}}(\mathbf{x_0})\frac{(\mathbf{x_0}-\mathbf{x_s})^T\mathbf{n}(\mathbf{x_0})}{|\mathbf{x_0}-\mathbf{x_s}|^2}\sqrt{2\pi|\mathbf{x_{ref}} - \mathbf{x_0}|} \times\left(\frac{8F_s}{7} + \frac{c}{|\mathbf{x_0}-\mathbf{x_s}|}\right),$$

$$T_{\mathrm{SW}}(\mathbf{x_0}, z) = z^{-\left[\!\left[F_s\frac{|\mathbf{x_0}-\mathbf{x_s}|}{c}\right]\!\right]}.$$

Four stages are clearly distinguished from equations (10) and (11): one independent of position and three dependent on loudspeakers and virtual source positions. The prefilter P, independent of the loudspeaker positions, can be computed once for all the loudspeakers. The filter F, scaling A, and delay T need to be computed sample by sample in real time. On incoming simulations, the following discretization parameters for equation (7) have been chosen: $K = 150$, $m = n = 5$ and $N = 25$. They return the half differentiator (Table 1) and the half integrator (Table 2) used as prefilter in (10) and (11).

Gain g	224.4994				
Zeros ζ_k	0.9854	0.8630	0.6078	0.2704	-0.0253
Poles π_k	0.9406	0.7510	0.4430	-0.1125	0.1077

Table1. Prefilter P_{PW} for the synthesis of a plane wave ($\alpha = 0.5$).

Gain g	0.0045				
Zeros ζ_k	0.9430	0.7624	0.4616	-0.1104	0.1199
Poles π_k	0.9860	0.8691	0.6243	0.2872	-0.0185

Table2. Prefilter P_{SW} for the synthesis of a spherical wave ($\alpha = -0.5$).

3. LOUDSPEAKER DISTRIBUTION

This section presents MATLAB simulations of the sound pressure field $P(\mathbf{x}, z)$, reconstructed with distributions of loudspeakers such as lines, circular arcs, squares and circles, and synthesized with the driving functions in (10) and (11). The synthesized sound fields in figures 2 and 4 have been computed using the following discrete-space form of the Kirchoff-Helmholtz integral:

$$P_{cont-time}(\mathbf{x}, \omega) = -\frac{\Delta \mathbf{x_0}}{4\pi} \sum_{l=0}^{L} D(\mathbf{x}_{0,l}, \omega) \frac{e^{-j\omega \frac{|\mathbf{x}-\mathbf{x}_{0,l}|}{c}}}{|\mathbf{x}-\mathbf{x}_{0,l}|}, \quad (12)$$

$$P_{disc-time}(\mathbf{x}, z) = -\frac{\Delta \mathbf{x_0}}{4\pi} \sum_{l=0}^{L} D(\mathbf{x}_{0,l}, z) \frac{z^{-\left[\!\left[F_s \frac{|\mathbf{x}-\mathbf{x}_{0,l}|}{c}\right]\!\right]}}{|\mathbf{x}-\mathbf{x}_{0,l}|}, \quad (13)$$

where $\mathbf{x}_{0,l}$ is the position of the lth loudspeaker and $\Delta \mathbf{x_0}$ is the distance between two adjacent loudspeakers that defines the spatial aliasing frequency $f_a = \mathrm{c}/\Delta \mathbf{x_0}$.

Figures 2 and 4 allow visual comparisons between analytical and discrete-synthesized fields for plane and spherical waves. It is clear from figure 2 that the rendering of spherical waves is more exact than the plane waves. Moreover, the rendering of spherical waves can be improved using a concave circular arc array, while for plane waves, a convex circular arc array does the work better. In this figure, in order to maintain the same *length* for line and circular arc arrays, the radius of curvature *R* and the angle of aperture φ for circular arc arrays have been chosen such that *length*=φR. Thus, given *length* and R, φ is straightforward.

On the other hand, figure 4 shows that in order to implement a closed listening area a square array or a circular array should be used. It can be seen in this figure that the synthesis of plane waves is improved with a circular array, where plane wave fronts appear more defined. Although the continuous-synthesized fields are not shown, tables 3 to 6 allows to compare those pressure fields over the listening area. Indeed, all percentage errors between continuous and discrete-time wave field synthesis (see Tables 3-6) have been computed using:

$$e_r(P_1, P_2) = \frac{|P_1 - P_2|}{|P_1|} \times 100\%. \quad (14)$$

4. DATA REGISTRATION

Monaural samples, recorded with omnidirectional and wind-shielded microphones, should be used with this reproduction scheme. It is preferable the use of a digital recorder with 24 quantization and capable of capturing at least 44100 samples per second. It is also strongly recommended to normalize the samples at -3dB and then to disappear the DC offset.

Once the collection of samples has been recorded, a spectral representation of the sound objects, [10], [11], should be done. This representation is very helpful to classify them in background and foreground sounds. For example, the spectrograms of a background sound such that the wind blowing through the trees have a smooth covering of all almost the whole time-frequency domain. This is not the case for example for the foreground sound of the song of a bird, whose spectrograms are composed of several increasing and decreasing curved lines referring to the fundamental and harmonic frequencies.

It is important to mention here that the reproduction of sound using spherical and plane wave models is widely used in room acoustics. Spherical waves are used for rendering of audio tracks such as music and speech, while plane waves are used for the rendering of room impulse responses, reproducing in that way the acoustics of a different room. Here, it is proposed another less known application for the composition and recreation of soundscapes. Since background sound are perceived as coming from a non-localized source and a foreground sound as from a localized source, their reproduction model appear in a natural respectively with plane and spherical wave models. For that, figure 6 shows the block diagram implementation of the driving function for each loudspeaker.

5. AURALIZATION OF NATURAL SOUNDS

Figure 6 presents a practical implementation of an immersive soundscape composed with natural sounds recorded in the highlands and beaches of Lima, Peru. Audio samples have been recorded using digital recorders such that the Sound Device 722 and the Sony PCMD50, both with an external, omnidirectional and wind-screened microphone. The multichannel auralization has been implemented using Pure Data, a real time audio processing language [12]. A graphical interface allows the composer to move up to five virtual sources over 24 audio channels, giving the spectator the sensation of being immerse in a natural scene due to the spatial component added to the piece of art.

A real system was developed in ISONAR Sound Research Workshop, at University of San Martin de Porres. It was presented for the first time in September 2009, during the "II Festival Lima Sonora", as part of a bigger event called "La semana del arte en Buenos Aires" [13]. The equipment used for this purpose was: one Mac Book Pro laptop, one M-audio Profire Lightbridge audio interface, three Behringer ADA8000 digital to analog converters, three QSC168X eight channel amplifiers, and 24 Behringer 1CBK loudspeakers (see figure 6).

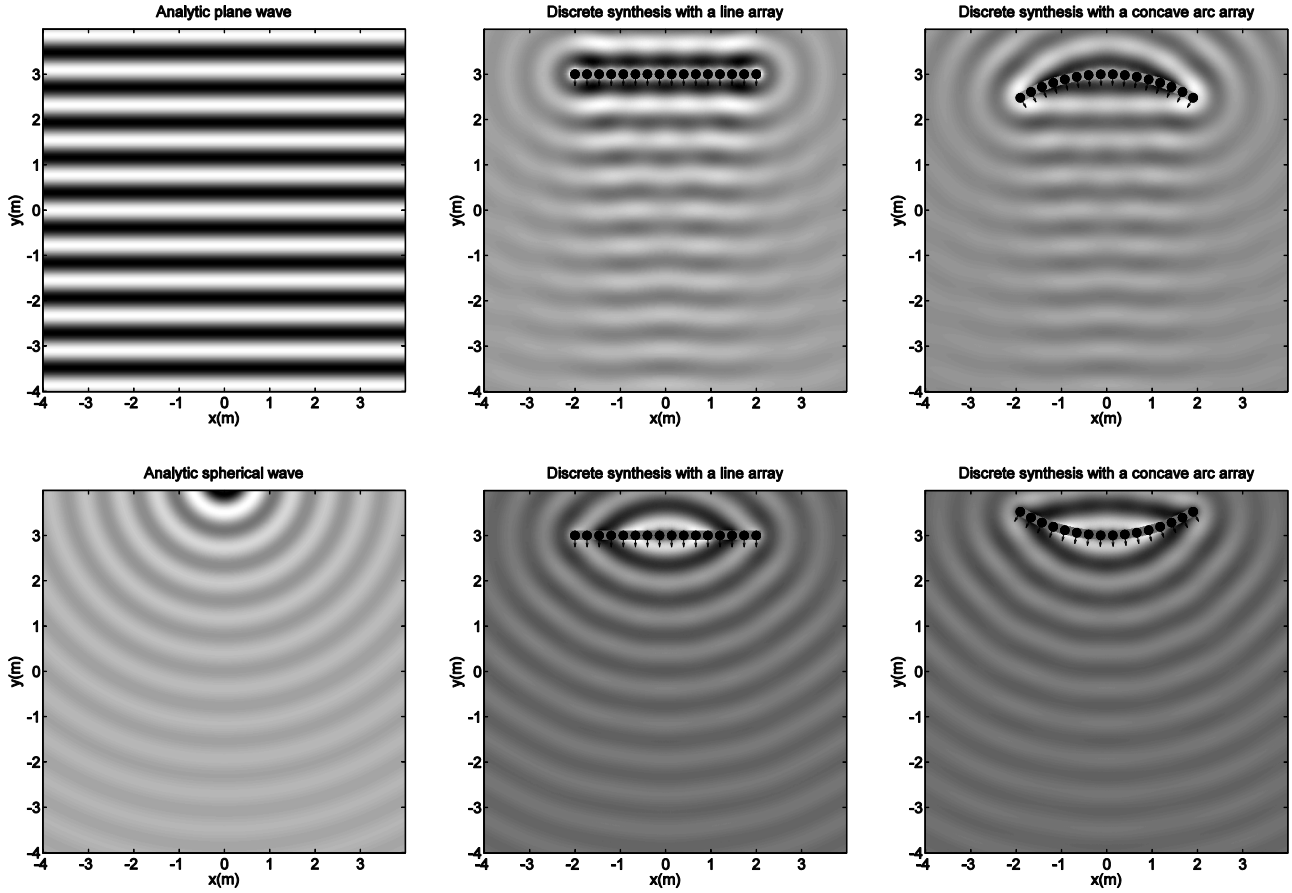

Figure2. Analytic (left) and discrete (center and right) wave fields synthesized with 16 loudspeakers. The source is a 440Hz pure tone. The plane wave direction is -90° and the spherical wave center is (0, 4.25m). The center of the line array is (0,3m). The distance between loudspeakers $\Delta\mathbf{x_0}$ is 17.4cm. The spatial aliasing frequency f_a is 1955Hz. In circular arc arrays, the radius of curvature is 3.75m. The listening area is 8x8m.

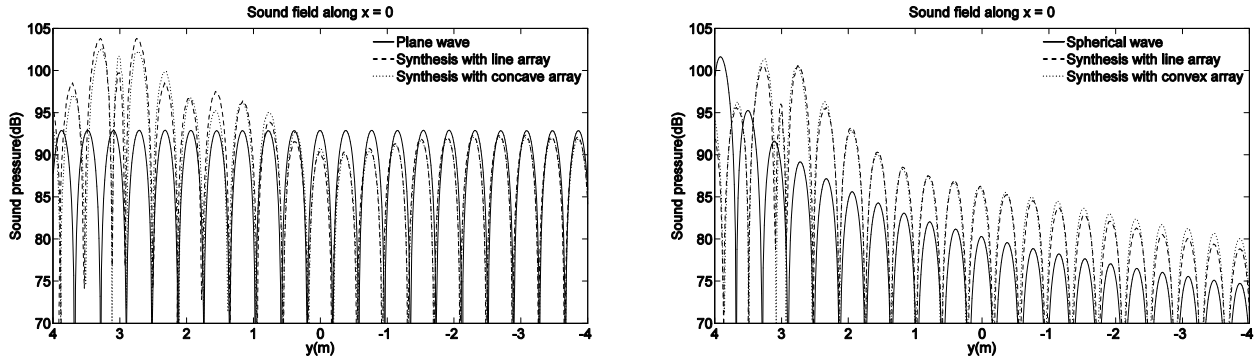

Figure3. Pressure decay in dB, in front of the loudspeaker arrays in figure 2 and along the line $x = 0$.

1	2	$e_r(P_1, P_2)$
Continuous – line	Discrete – line	00.44%
Continuous – concave	Discrete – concave	01.43%
Continuous – convex	Discrete – convex	01.45%

Table3. Percentage errors of continuous to discrete sound field synthesis along $x = 0$. The plane wave is reconstructed using 16 loudspeakers distributed in line, concave arc and convex arc arrays.

1	2	$e_r(P_1, P_2)$
Continuous – line	Discrete – line	2.94%
Continuous – concave	Discrete – concave	2.45%
Continuous – convex	Discrete – convex	5.10%

Table4. Percentage errors of continuous to discrete sound field synthesis along $x = 0$. The spherical wave is reconstructed using 16 loudspeakers distributed in line, concave arc and convex arc arrays.

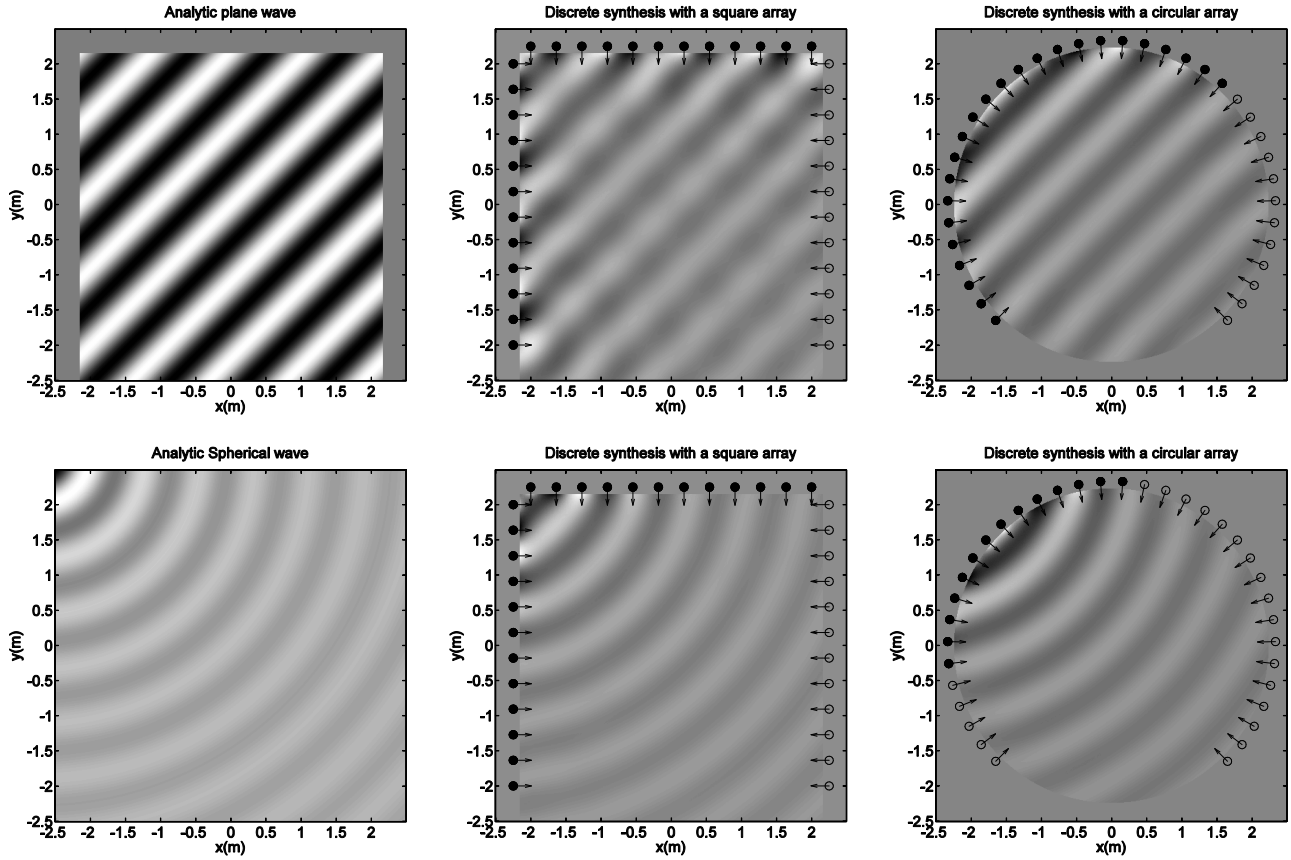

Figure4. Analytic (left) and discrete (center and right) wave fields synthesized with 36 loudspeakers. The source is a 440Hz pure tone. The plane wave direction is -45° and the spherical wave center is (-2.75, 2.75m). In the square array the distance between loudspeakers $\Delta\mathbf{x_0}$ is 36.6cm, and the spatial alias frequency f_a is 905 Hz. In the circular array the radius of curvature is 3.75m, the distance between loudspeakers $\Delta\mathbf{x_0}$ is 31.4cm, and the spatial alias frequency f_a is 1081 Hz.

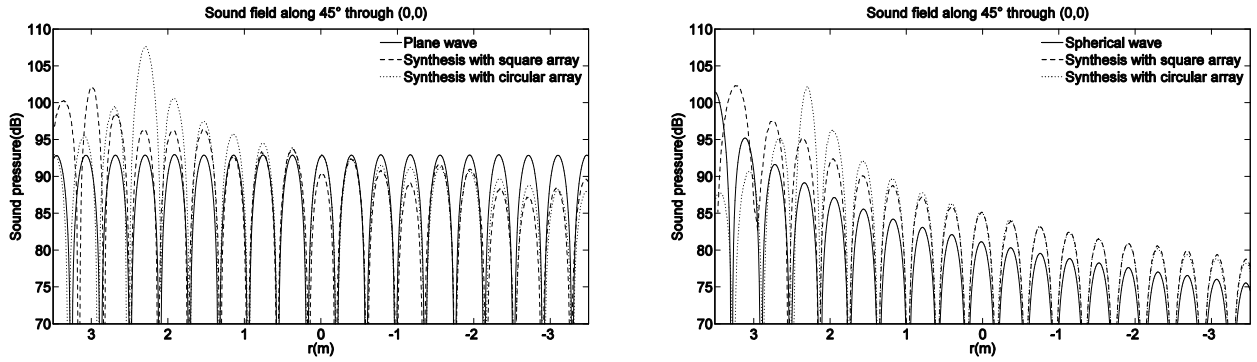

Figure5. Pressure decay in dB, inside the listening area in figure 4 and along the line passing through (0,0) with 45° inclination.

1	2	$e_r(P_1, P_2)$
Continuous – square	Discrete – square	1.46%
Continuous – circular	Discrete – circular	1.44%

Table5. Percentage errors of continuous to discrete sound field synthesis in the whole listening area. A plane wave is reconstructed using 36 loudspeakers distributed in square and circular arrays.

1	2	$e_r(P_1, P_2)$
Continuous – square	Discrete – square	3.10%
Continuous – circular	Discrete – circular	3.22%

Table6. Percentage errors of continuous to discrete sound field synthesis in the whole listening area. A spherical wave is reconstructed using 36 loudspeakers distributed in square and circular arrays.

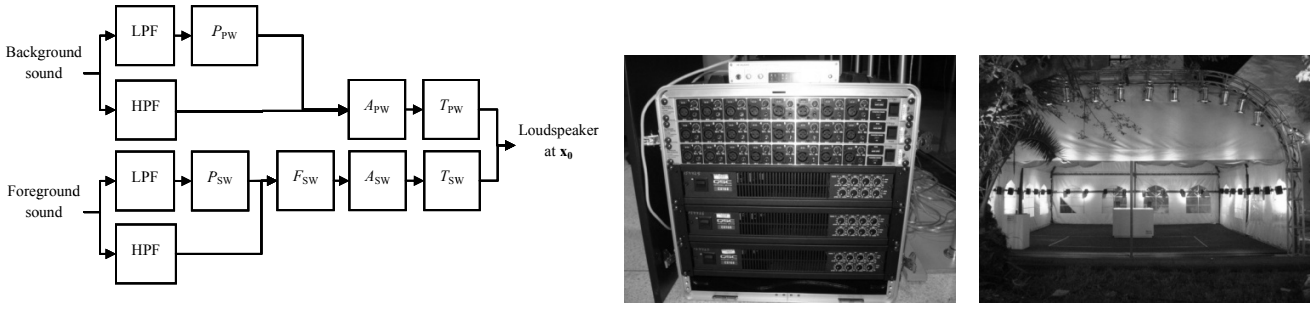

(a) (b) (c)

Figure6. The system for the auralization of natural sounds is composed of: a) The real-time driving function computations for each loudspeaker, b) the audio interface between computer and loudspeakers and c) the virtual auditory scene with 24 loudspeakers that defines an 8x8m listening area.

6. CONCLUSIONS

This paper presented a complete description of the implementation of an immersive soundscape. It began with a discrete fractional-order zero-pole formulation of the generalized continuous wave field synthesis method, followed by the appropriate simulations for the selection of a suitable loudspeaker distribution.

It has also been proposed a non-typical application of the WFS method for the composition and recreation of immersive soundscapes. Indeed, the rendering of foreground and background sounds using plane and spherical wave models, respectively. Simulations of a real case report a discretization percentage error around 1%, using 24 loudspeakers and a 5^{th} order IIR pre-filter per channel.

As an example, it has been described a real immersive soundscape which has been shown in a public exhibition. It is important to mention here that the auralization can be improved with the following steps: a) the modeling of the loudspeakers distribution selection problem according to the geometry of the room, and b) the synthesis of directional and focused sources for the auralization of virtual sources inside the listening area.

7. ACKNOWLEDGMENTS

The author would like to thanks people from ISONAR Sound Research Workshop and from Research Department, both at University of San Martin de Porres, for financial support during this project. He would like to thank people from ECOS Sound Research Group for their valuable ideas. He also would like to thank Prof. Paul Rodriguez and Prof. Andres Flores from Pontifical Catholic University of Peru, and MSc. Chris Tomás from Universidade Federal do Rio Grande do Sul, to all of them for their reviews of this paper.

8. REFERENCES

[1] Berkhout, “A holographic approach to acoustic control,” in *Journal of the Audio Engineering Society*, vol. 36, no. 12, december 1988, pp. 977-995.

[2] Berkhout, D. de Vries and P. Vogel, “Acoustic control by wave field synthesis,” in *Journal of the Acoustic Society of America*, vol. 93, no. 5, may 1993, pp. 2664-2778.

[3] M. Schafer, *The tuning of the world*. Knopf, New York, USA, 1977.

[4] S. Spors, J. Ahrens and R. Rabenstein, “The theory of wave field synthesis revisited,” in *124th Audio Engineering Society Convention*, Amsterdam, The Netherlands, May 2008.

[5] M. Al-alaoui, “Novel digital integrator and differentiator,” in *Electronics letters*, vol. 29, 1993, pp. 376-378.

[6] M. Al-alaoui, “Al-alaoui operator and the new transformation polynomials for discretization of analogue systems,” in *Electronic Engineering*, Springer-Verlag, vol. 90, 2008, pp. 455-467.

[7] K. Oldham and J. Spanier, *The fractional calculus*. Academic Press, New York, USA, 1974.

[8] R. Barbosa, J. Tenreiro Machado and I. Ferreira, “Pole-zero approximations of digital fractional-order integrators and differentiators using signal modeling techniques,” in *Proceedings of the 16th IFAC World Congress*, Prague, Czech Republic, July 2005.

[9] R. Barbosa and J. Tenreiro Machado, “Implementation of discrete-time fractional-order controllers based on LS aproximations,” in *Acta Polytechnica Hungarica*, vol. 3, no. 4, 2006, pp. 5-22.

[10] P. Schaeffer, *Traité des objets musicaux*. Seuil, Paris, France, 1988.

[11] M. Chion, *El sonido: música, cine, literatura.* Paidós, Barcelona, España, 1999.

[12] Pure Data: http://www.puredata.org

[13] Lima Sonora: http://www.limasonora.com